LABORATORI NAZIONALI DI FRASCATI
SIS – Pubblicazioni

LNF–99/019 (P)
19 Luglio 1999

Order-disorder in Olivine Minerals by Synchrotron X-ray Absorption Near-edge Structure (XANES) Spectroscopy at the Mg, Fe and Ca K Edges

Ziyu Wu[1], Annibale Mottana[1,2], Eleonora Paris[3], Gabriele Giuli[3], Augusto Marcelli[1], and Giannantonio Cibin[1]

[1]Istituto Nazionale di Fisica Nucleare, Laboratori Nazionali di Frascati
P.O. Box 13, I-00044 Frascati RM, Italy
[2]Dipartimento di Scienze Geologiche, Università Roma Tre
Largo S. Leonardo Murialdo 1, I-00146 Roma RM, Italy
[3]Dipartimento di Scienze della Terra – INFM, Università di Camerino
Via Gentile III da Varano, I-62032 Camerino MC, Italy

Abstract

Synchrotron Mg and Fe X-ray absorption near-edge K XANES spectra of the Pbnm olivine series endmembers forsterite (Mg_2SiO_4), fayalite (Fe_2SiO_4), monticellite ($CaMgSiO_4$) and kirschsteinite ($CaFeSiO_4$), as well as of the intermediate member of the Fe-Mg olivine solid solution series "hortonolite" ($MgFeSiO_4$), have been recorded experimentally and calculated by the multiple-scattering theory using clusters of different size and the Xα exchange-correlation potential. Comparison of experimental and theoretical spectra shows that all transition features, energy positions and relative intensities can be reproduced in the energy range up to 60 eV above threshold when using clusters containing at least 80 atoms and extending over a sphere at least 0.6 nm in radius away from the absorber. It also indicates that, at the XANES sensitivity level, Mg and Fe are located entirely in the expected structural sites in all four endmembers, and distribute in "hortonolite" following a regular order, however with no clear preference for either octahedral site. Thus, atomic order-disorder on a short- to medium-range scale can be detected by the XANES method, hence contributing to understanding the behavior of these materials. The Ca K-edge spectra of monticellite and kirschsteinite have been recorded and calculated too; they are consistent with the assignment of all Ca to the M2 site and confirm that all endmembers of the Pbnm olivine family match the octahedral cation distributions indicated by the ideal crystal structure.

PACS.: 78.70.Dm, 81.40.P
Key words: x-ray absorption, spectroscopy, omphacite, sincrotron, magnesium, aluminium

Submitted to American Mineralogist

INTRODUCTION

Olivines, M2M1[TO_4]-Pbnm, are compounds of geological and geophysical importance as they are widespread all over the oceanic crust and upper mantle of the Earth. In the igneous realm, Fe-Mg olivines are early crystallization products from primary basaltic magmas in the Earth and Earth-like planetary bodies (Poirier 1991). In the metamorphic realm they occur in mafic and ultramafic rocks as the high-grade dehydration and re-equilibration products of serpentines (Valley and Essene 1980). Ca-olivines are occasionally found in contact-metamorphic bodies and skarns (Tracy and Frost 1991) and exceptionally in meteorites as low-temperature re-equilibration products (Folco and Mellini 1997). The Pbnm (or α) olivine crystal structure is indeed very frequently found in compounds with A_2BX_4 stoichiometry (where A, B are cations, and X anions of various size and valence: e.g., Muller and Roy 1974; Lumpkin and Ribbe 1983; Hazen and Finger 1987).

Most crystal-chemical studies are devoted to the octahedral A cations (also labeled M = Mg, Fe, Ca and minor ones such as Ni, Co, Mn, Li, etc.), whilst the tetrahedral B cation (Si in silicate olivines, but also Ge, Be, etc.) is investigated less because of its alleged character of "hard sphere". Until some time ago crystal-chemical studies especially concerned the long-range order of cations (LRO) and were carried out by X-ray or neutron diffraction (e.g., Motoyama and Matsumoto 1989; Ottonello et al. 1990; Artioli et al. 1995; Henderson et al. 1996; Redfern et al. 1997). A detailed knowledge that included their short-range order (SRO) was not available, although it was a prerequisite to assess the olivine chemical and physical properties as well as behavior when submitted to the changing P,T conditions on and in the Earth (e.g., Kieffer 1979; Hofmeister 1987; Williams et al. 1990; Chakraborty 1997). Only the question of Mg vs. Fe partitioning over the two non-equivalent M1 and M2 structural sites in the silicate olivine solid-solution series was investigated frequently since it represented an important application of the Mössbauer effect (ME), but without reaching consensus (e.g., Virgo and Hafner 1972; Aikawa et al. 1985; Akamatsu and Kumazawa 1993). Indeed, some uncertainties inherent single-crystal X-ray diffraction structure refinement (SC-XRef), the method of investigation that enjoys preference over all others, often make its results inconsistent with those derived from other experimental methods, including ME (Kirfel 1996). Consequently, even greater discrepancies arise with methods that are theoretical in approach (e.g., Alberti and Vezzalini 1978; Iishi 1978; Ottonello 1987; Pilati et al. 1990, 1995; Brodholt 1997). As a matter of fact, solid solutions can be studied by SC-XRef with less proficiency than compositions close to endmembers because their inherent structural disorder varies unpredictably, so as to often hinder precise site occupancy measurements.

By contrast, X-ray absorption spectroscopy (XAS) is a powerful tool to gain information on order-disorder in solid materials, being both an atom-selective and a local probe (Bianconi 1988; Durham 1988). However, only recently could we present a theoretical study (Wu et al. 1996a) on the Mg and Fe K-edge X-ray absorption near-edge structures (XANES) at room temperature and under extreme conditions for forsterite (Fo: Mg_2SiO_4) and fayalite (Fa: Fe_2SiO_4), the endmembers of the Fe-Mg olivine series. That study mainly had the purpose of testing the validity of our theoretical models as well as the effectiveness of our calculation method, but in that way we could also show that an independent structural study is feasible.

In this paper, we present new, high-resolution experimental spectra at the Mg and Fe K edges for the two Fe-Mg endmembers Fo and Fa, and for three other olivines. Two are the Ca endmembers of the family, namely monticellite (Mtc: $CaMgSiO_4$) and kirschsteinite (Krs: $CaFeSiO_4$). The third one is the intermediate 1:1 member of the Fo-Fa solid solution series known under the variety name "hortonolite" (Hrt: $MgFeSiO_4$), which we have taken as model compound to address the problem of Mg-Fe order-disorder in the whole olivine series. We will first compare experimental spectra at the Mg and Fe K edges with their theoretical equivalents; then simulate different ordering patterns and compare the calculated spectra with the experimental ones.

The main purpose of this work is to investigate the effects of Mg, Fe, and Ca partition in the Pbnm (or α) olivine structure on the electronic properties, as well as the relationships that exist between chemical substitutions and features occurring in XANES spectra. In addition, we want to explore the relationships that intervene between LRO, as determined by XRD, and SRO, as determined by XANES, on the endmembers and on a well-known intermediate member as well, and deduce from it a model for the behavior of the entire olivine solid-solution system.

MATERIALS AND METHODS

Samples

Chemical compositions and crystal data for the measured olivines and for those used as reference are given in Tables 1 and 2, respectively, together with the nominal compositions of synthetic endmembers.

Table 1 – Chemical compositions (wt.%) of the olivines: theoretical endmembers, actually measured by XAS (*) and taken from literature (†) to be used as reference.

Sample	SiO2	FeO	MnO	MgO	CaO	sum	
Fo	42.71	---	---	57.29	---	100.00	
Fo1a	41.79	0.16	0.08	56.32	0.01	98.36	(*)
Fo1a	41.79	0.16	0.08	56.32	0.01	98.36	(*)
FNJ	33.28	44.15	5.70	16.66	n.d.	99.79	(†)
Fa	29.50	70.50	---	---	---	100.00	(*)
Mtc	38.40			25.75	35.85	100.00	
Mo2a	37.30	3.78	0.48	23.20	35.18	99.94	(*)
Krs	31.96	38.21			29.83	100.00	(*)
KIR1	31.96	38.21			29.83	100.00	(†)

Note:
Fo1A: natural sample from Afghanistan
FNJ: natural sample from Franklin (Smith and Hazen 1973; Hazen 1977)
Mo2A: natural sample from Magnet Cove AK (includes REE n.d.)
KIR1: meteorite from Vulcano Laziale (Folco and Mellini 1997)

Table 2. Crystal data (nm) of olivines used as input to calculate the theoretical K-edge spectra.

Forsterite (Fo1A: Afghanistan; F. Demartin, pers. communication)
a = 0.47560(4), b = 1.02060(6), c = 0.59856(6), V = 0.29054

atom	**x/a**	**y/b**	**z/c**
M1	0	0	0
M2	-0.00837(4)	0.27737(2)	0.25
Si	0.42647(3)	0.09403(1)	0.25
O1	-0.23386(8)	0.09154(3)	0.25
O2	0.22180(7)	0.44697(3)	0.25
O3	0.27757(5)	0.16308(2)	0.03294(4)

Hortonolite FNJ (Franklin; Hazen 1977)
a = 0.4798(5), b = 1.039(1), c = 0.6055(6), V = 0.3018

atom	**x/a**	**y/b**	**z/c**
M1	0	0	0
M2	0.9867(1)	0.2792(1)	0.25
Si	0.4287(2)	0.0957(1)	0.25
O1	0.7661(5)	0.0918(2)	0.25
O2	0.2127(6)	0.4514(2)	0.25
O3	0.2844(4)	0.1633(2)	0.0357(3)

Fayalite (synthetic; Fujino et al. 1981)
a = 0.48195(6), b = 1.04788(17), c =0.60873(8), V = 0.30742

atom	**x/a**	**y/b**	**z/c**
M1	0	0	0
M2	0.98598(5)	0.28026(2)	0.25
Si	0.43122(10)	0.09765(5)	0.25
O1	0.76814(23)	0.09217(12)	0.25
O2	0.20895(25)	0.45365(11)	0.25
O3	0.28897(17)	0.16563(9)	0.03643(9)

Monticellite (Mo2A: Magnet Cove; F. Demartin pers. communication)
a = 0.48306(5), b = 1.11138(14), c = 0.63916(5), V = 0.3431

atom	**x/a**	**y/b**	**z/c**
M1	0	0	0
M2	-0.02246(2)	0.27683(1)	0.25
Si	0.41098(7)	0.08159(1)	0.25
O1	-0.25389(8)	0.07790(4)	0.25
O2	0.24570(8)	0.44902(4)	0.25
O3	0.27347(6)	0.14776(2)	0.04553(4)

Kirschsteinite (KIR1: Vulcano Laziale; Folco and Mellini 1997)
a = 0.4877(1), b = 1.1166(1), c = 0.6448(1), V = 0.3511

atom	**x/a**	**y/b**	**z/c**
M1	0	0	0
M2	0.98072(5)	0.27719(2)	0.25
Si	0.41609(6)	0.08437(3)	0.25
O1	0.7490(2)	0.0802(1)	0.25
O2	0.2344(2)	0.4515(1)	0.25
O3	0.2816(1)	0.1507(1)	0.0475(1)

Forsterite (Fo1a) is a colorless transparent crystal implanted on calcite and lazurite in a marble from Afghanistan. Monticellite (Mo2a) is a coarse mosaic aggregate with calcite in a marble from Magnet Cove AR. The fine-grained powders of both natural samples were purified

by hand picking under the binocular microscope and rapidly cleansed with very dilute HCl to avoid damage. Three other samples are synthetic and obtained in two different ways, however with identical results. Reagents (suprapure SiO_2, Fe_2O_3, MgO, and $CaCO_3$) were finely mixed, fired, pressed into pellets, run at 1100 to 1300 °C for 24 h at room pressure in a vertical furnace under the steady flow of a 80:120 ml/min gas mixture of $CO+CO_2$, and finally quenched in dry ice after cooling first to 900 °C to avoid oxidation. Syntheses were also run directly in a piston-cylinder apparatus at 1 GPa and 1500 °C in Fe capsules. In both cases, complete synthesis was achieved for Fa and Hrt. The Krs mix did not turn into crystals at once. The first trial gave way to a porous olivine + silica mixture bound by glass of hedenbergite composition; this mixture had to be ground and run again three times before turning into a homogeneous crystalline single phase.

XAS Measurements

Experimental K-edge spectra for Mg and Fe were recorded at Stanford Synchrotron Radiation Laboratory (SSRL), using synchrotron radiation (SR) emitted by SPEAR, that operates at 3.0 GeV with maximum current 100 mA and typical lifetime 20 h. For Mg we used beamline SB03-3, where the JUMBO monochromator is equipped with YB_{66} crystals (Wong et al. 1994). The spectra were collected in vacuum in the total yield (TEY) mode (Erbil et al. 1988; Gudat and Kunz 1977) at steps of 0.3 eV and with a resolution estimated to be 0.55 eV (Schaefers et al. 1992). For Fe we used beamline SB04-1, and a double-crystal monochromator with Si (111), the experimental resolution being 1.5 eV. The spectra were acquired in the fluorescence yield (FEY) mode at steps of 0.35 eV for 1 s using a Lytle detector and Soller slits and with the sample compartment filled by He (Lytle et al. 1984). The powdered samples were glued directly on an Ag-coated Al holder in the first set-up, and spread evenly onto a kapton tape in the second one. In both set-ups, holders were oriented at a 45° angle to the impinging SR beam.

The Ca spectra were recorded at LURE, Orsay, France, at beamline D44, with DCI operating at 1.85 GeV and 100~200 mA positron current. They were collected in the transmission mode in air, using a channel-cut Si (311) crystal as monochromator, with energy resolution 1.4 eV (Galoisy and Calas 1992). Standard Ti foil was used for energy calibration. Spectra were recorded at 0.5 eV steps and counting time 3 s from powders deposited on kapton tape.

XANES Calculations

Theoretical spectra were calculated at INFN-LNF by the CONTINUUM code (Natoli et al. 1980, 1990; Tyson et al. 1992; see also Durham et al. 1982; Durham 1988; Rez et al. 1995) which is based on the full multiple-scattering (MS) theory (Lee and Pendry 1975) and has been widely used to interpret XANES spectra in a variety of systems, including some which are similar to the present one (e.g., Wu et al. 1996a,b; Mottana et al. 1997, 1999). We follow Mattheiss (1964) prescription to construct the cluster density, and obtain the Coulomb part of the potential by superimposition of tabulated neutral atomic charge densities (Clementi and Roetti 1974). In order to simulate the charge relaxation around the core hole in the photoabsorber of atomic number Z, we use the well-screened Z+1 approximation (final state

rule: Lee and Beni 1977). This consists of taking the orbitals of the Z+1 atom and constructing the charge density by the excited electronic configuration of the photoabsorber with the core electron promoted to the lowest empty orbital. For the exchange correlation part of the potential we use the energy-independent Xα type of exchange (Slater 1979) because it proved more flexible than the Hedin-Lundqvist (1971) potentials and is especially suitable for insulating materials. We have chosen the muffin-tin radii according to the criterion of Norman (1974) and allowed a 10% overlap between contiguous spheres to simulate the atomic bond. The calculated spectra are further convoluted with a Lorentzian shaped function, with a full width Γ 0.36 eV for the Mg K edge and 0.40 eV for the Fe K edge to account for core hole lifetime (Fuggle and Inglesfield 1992 appendix B p. 347; Penn 1987; Krause and Oliver 1979), and with Γ_{exp} 0.55 viz. 1.5 eV for experimental resolutions. Features will be discussed in the light of our strategy of MS calculation that makes use of clusters of progressively increasing size and number of atoms around the excited atom until reaching convergence in two successive cycles.

RESULTS AND DISCUSSION

Experimental spectra at the various K edges will be first reported and described, then interpreted starting from the crystal structure data of the related reference phases (as determined by SC-XRef) with the aid of the theoretical spectra calculated from them.

Mg and Fe K edges

The experimental Mg K-edge XANES spectra for forsterite, “hortonolite” and monticellite are shown in Fig. 1. All spectra show four gross features that are qualitatively similar both in the edge region (Bianconi 1988; also named full-multiple-scattering region, FMS, by Natoli and Benfatto 1986) i.e., up to +15 eV above threshold, and in the XANES region (or intermediate-multiple-scattering region, IMS) that in these systems goes from +15 to +60 eV above threshold.

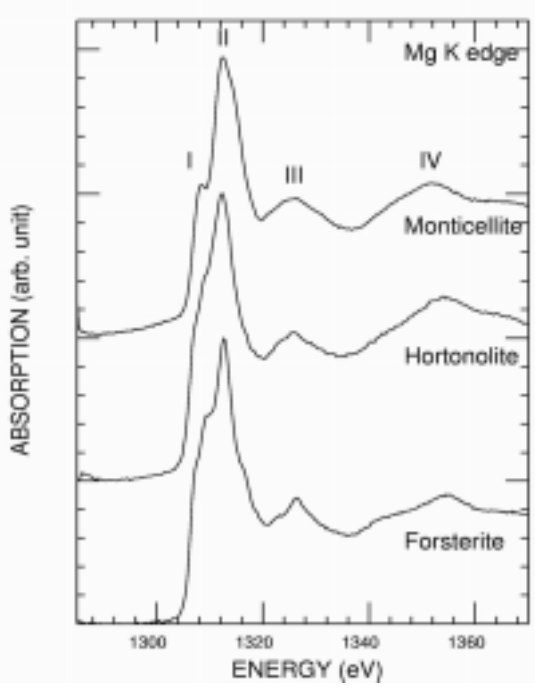

Figure 1 – Experimental Mg K-edge XANES spectra for forsterite, “hortonolite”, and monticellite.

Indeed all three compounds have their Mg atoms set within first coordination shells that are similar (six O atoms) and with the same point-group site symmetries (4a for M1 and 4c for M2). However, individual spectra have differences that are most evident in the edge region, where Fo clearly exhibits a number of fine structures (arrows) that can only barely be seen in Hrt, and even less in Mtc (Fig. 1). Fine structures superimposed on the gross features can be evidenced also in the IMS regions and will be used to gather preliminary information on the amount of structural disorder in the systems. On the basis of the number of fine structures Fo is slightly more ordered than Hrt, and both are considerably more ordered than Mtc. As a matter of fact, the Mtc spectrum shows very few fine structures and practically consists of the four gross features only.

In Fo, the M1 and M2 sites are fully occupied by Mg only. SC-XRef (Table 2; cf. also Fujino et al. 1981) informs that they differ in point symmetry (M1 has 1 and M2 m) and mean size (<M1-O> = 0.2094, <M2-O> = 0.2129 nm) while being substantially equivalent in edge length distortion as estimated by the octahedral quadratic elongation parameter, OQE (Robinson et al. 1971): OQE_{M1} = 1.0269, OQE_{M2} = 1.0260. They show small differences only in their octahedral angle variances, OAV (Robinson et al. 1971): OAV_{M1} = 94.8, OAV_{M2} = 89.7. In Mtc (Table 2; cf. also Pilati et al. 1995; Sharp et al. 1987) only site M1 is believed to contain Mg. This site is slightly larger (<M1-O> = 0.2136 nm) and considerably more distorted (OQE = 1.0287, OAV = 104.0) than either of the two Fo sites. By contrast, the large (<M2-O> = 0.2373 nm) and very distorted (OQE = 1.0481, OAV = 165.7) M2 site is the one preferred by Ca. As for Hrt, the rare SC-XRef data available at present were made on natural samples which contain considerable amounts of impurities, especially Mn (Table 1; cf. Hazen 1977; Smyth and Hazen 1973; Brown and Prewitt 1973). They indicate (Table 2) that the M1 and M2 sites (both larger than those corresponding to Fo) are comparable in their sizes (<M1-O> = 0.2135 nm and <M2-O> = 0.2167 nm) and distortions, with identical elongations (OQE_{M1} = 1.033, OQE_{M2} = 1.034) and angle variances not significantly different (OAV_{M1} = 119.3, OAV_{M2} = 114.3). Thus, no a priori conclusion on their relative Mg vs. Fe content is warranted.

SC-XRef information does not appear to meet entirely the evidence contained in our experimental Mg K-edge spectra. In the IMS region of the Fo spectrum, the presence of two M sites occupied by Mg is made evident by the doubling of most, if not all, gross features, with the highest-in-energy fine structure always referring to Mg in M1, the smallest site, according to Natoli's rule (Natoli and Benfatto 1986). The Hrt spectrum is consistent with that of Fo in that it also shows its features doubled. The Mtc spectrum is rather broad but it is not doubled, as expected, since only the M1 site is suitable to host Mg. Nevertheless, even in this spectrum an explanation must be sought for the two additional features shown as arrows in Fig. 1. Note, moreover, that the Mtc fourth gross feature shows a negative energy shift relative to the corresponding features for both Fo and Hrt (-4 eV) which is consistent with the SC-XRef result that the site available for Mg in this mineral is larger than the M1 site in both Fo and Hrt (see later).

For Hrt too, XANES and SC-XRef give results that are mutually inconsistent: on one hand, according to SC-XRef both the M1 and the M2 sites of this compound are just as large as the M1 site of Mtc (see above); on the other hand, the energy of the fourth XANES feature

suggests that the Hrt octahedral site is as large as the Fo M1 site, but smaller than the Mtc one. The two techniques lead to different results because SC-XRef integrates information from all Fe and Mg atoms, thus giving as a result an average octahedron, whereas XANES, being element-specific, tells us about the size of the octahedron that surrounds Mg only. Even when taking into account the fine structure on the raising limb of the fourth gross feature, which might be interpreted as suggesting that some Mg enters a second, large M site, we argue that, in our synthetic Hrt sample, most Mg enters a polyhedron having the same geometrical constraints as the Fo M1 octahedron, thus absorbing X-rays at the same energy. Conversely, a complementary amount of Fe, if any, should move to the other octahedron so that the 1:1 stoichiometry is restored. Thus, in order to find support for this interpretation we must look for information in the Fe K-edge spectrum.

The experimental Fe K-edge spectra for fayalite, "hortonolite", and kirschsteinite are given in Fig. 2. They too show four gross features, as the Fe site symmetries are the same as for Mg (see above). However, the first gross feature is now a shoulder that almost disappears under the raising limb of the major one and, in addition, the entire Fe XANES region is much less finely structured than the Mg one was.

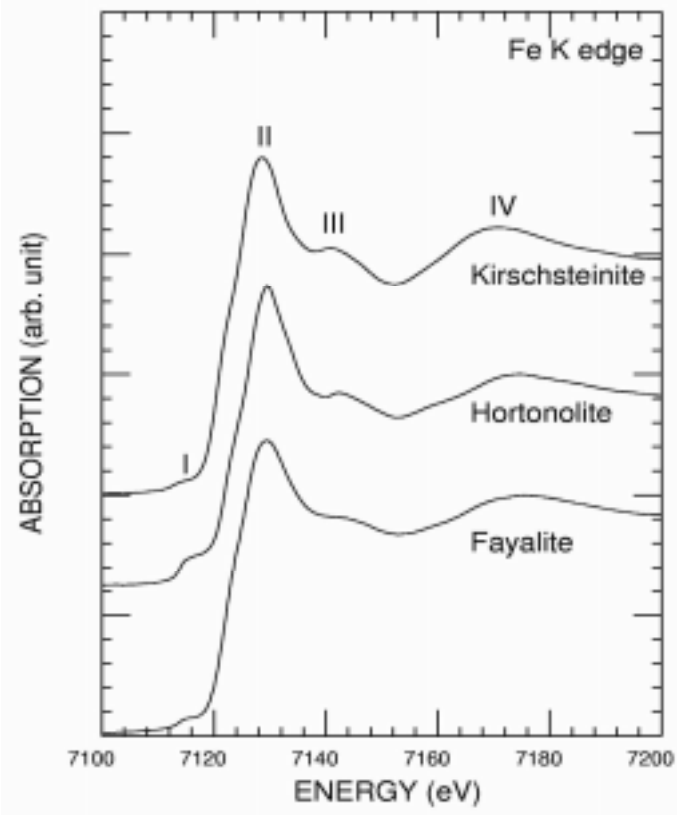

Figure 2 – Experimental Fe K-edge XANES spectra for fayalite, "hortonolite", and kirschsteinite.

These spectral properties can easily be explained. In Fa, both sites are occupied by Fe2+ and are therefore larger than the corresponding Mg sites of Fo (Table 2: Fujino et al. 1981); however they are very similar one to the other as for their sizes (<M1-O> = 0.2161, <M2-O> = 0.2177 nm) and edge distortions (OQE_{M1} = 1.0379, OQE_{M2} =1.0370). They differ a little, but not significantly, only in their angle variances (OAV_{M1} = 130.1, OAV_{M2} = 124.9). In Krs (Table 2; cf. Folco and Mellini 1997), the large site M2 is assumed to be taken over entirely by

Ca (<M2-O> = 0.2368 nm) as in Mtc, and the much smaller M1 site (<M1-O> = 0.2181 nm) by Fe2+. Both sites display significant distortions, in elongation (OQE_{M1} = 1.035, OQE_{M2} = 1.049) as well as angle (OAV_{M1} = 168.8, OAV_{M2} = 123.7). However, the Krs and Fa spectra are rather similar, with the former better resolved than the latter, also at the pre-edge. Furthermore, the negative energy shifts of features III and V indicate that the iron site in Krs is larger than both those that Fe occupies in Fa (and in Hrt as well, whichever this site may be). The energy displacement is greater than in Mtc (8 eV: Fig. 2) because Fe absorbs at higher energy than Mg, but this finding simply brings additional, indirect support to what had been already observed in the Mg spectrum and to the ensuing interpretation (see above).

As a matter of fact, the Fa features result from superposition of two similar, but non-identical Fe contributions, as it was the case for Mg in Fo. Therefore it is surprising that our synthetic Fa, being chemically pure, gives rise to a Fe K-edge spectrum that is simpler and less resolved, or at least not as well-resolved as Mg in Fo. Moreover, the Fa spectrum also displays the weakest pre-edge and third feature (Fig. 2), thus showing greatest disorder among all the given Fe K-edge spectra. This experimental finding supports a previous inference of ours (Wu et al. 1996a) about synthetic Fa showing poor Fe spectra because it is structurally poorly organized as a result of defects acquired during crystal growth (cf. Nakamura and Schmalzried 1983).

Surprisingly, neither the Fa Fe K-edge spectrum nor the Krs one are as sharp and strong as the Hrt spectrum: note, in particular, how strong the absorption jump and the pre-edge peak are, and the sharpness of the third feature in this intermediate compound (Fig. 2). Indeed the Hrt spectrum is the best structured among all i.e., it is the one showing greatest order around the site occupied by iron. Additional work on this compound is again needed, the more so because our Fe K-edge analysis somewhat contradicts the evidence arising from its Mg K edge. A comparison between Fig. 1 and Fig. 2 might even suggest that a relationships exists between type of atom and local order: this appears to increase with increasing atomic number (Fe), or decrease in light element (Mg) content of the site.

In order to clarify the matter and obtain definitive information on the location of the Mg and Fe atoms in Hrt (i.e., in a 1:1 Fo-Fa solid solution where the problem of order-disorder is still unresolved by other methods), we made up our mind to start from the beginning and study everything anew, the endmembers first. So, calling to mind the property of XANES of being chemically selective (i.e., able to give information about Mg independently upon Fe), we began with computing separately the theoretical spectra for the two endmembers by convoluting the relevant component cluster spectra.

In Fig. 3 we report the calculated Mg K-edge spectra for individual clusters centered at the M1 (left panel) and M2 (middle panel) sites of Fo, the prototype, and computed for shells which increase stepwise in radius by 0.1 nm thus incrementing the numbers of their atoms, till convergence. The convergent clusters include no less than five shells and as many as 89 atoms (31 Mg + 10 Si + 48 O) to within a distance of 0.58~0.62 nm from the Mg atom taken as absorber at the center of each cluster: M1 (left) and M2 (middle). This calculation confirms our previous one (cf. Fig. 2 in Wu et al. 1996a); the very minor differences are due to the fact that we now make use of the Xα type of exchange, against the Hedin and Lundqvist's potentials we

had used at that time. Our first-shell spectra for the M1 and M2 sites (Fig. 3: curves **a** are quite similar, because the short-range environments are the same (1 Mg + 6 O) and differences in the individual bond lengths are minor. Both calculations give rise to a relatively sharp and strong feature at +4 eV above threshold. In terms of scattering, this feature should be understood as arising from intra-shell multiple scattering of the photoelectron emitted by Mg within the first coordination shell of six O atoms. It may also be seen as the result of the caging effect of such a small oxygen shell on the excited photoelectron: back scattering creates a relatively sharp scattering resonance around the photoabsorber. This is in agreement with several previous works; e.g., on NiO (Vvedensky and Pendry 1985), MgO (Lindner et al. 1986; Wu et al. 1996a) and MnO (Kurata et al. 1993). In Fig. 3, curves **a** show another broad peak at higher energy (+42 eV) that reproduces the fourth gross feature of the experimental spectrum. This peak, that is generated when only using the first shell of six O atoms, arises from dominantly single-scattering events within this shell; thus, it is this IMS structure that informs about short-range order.

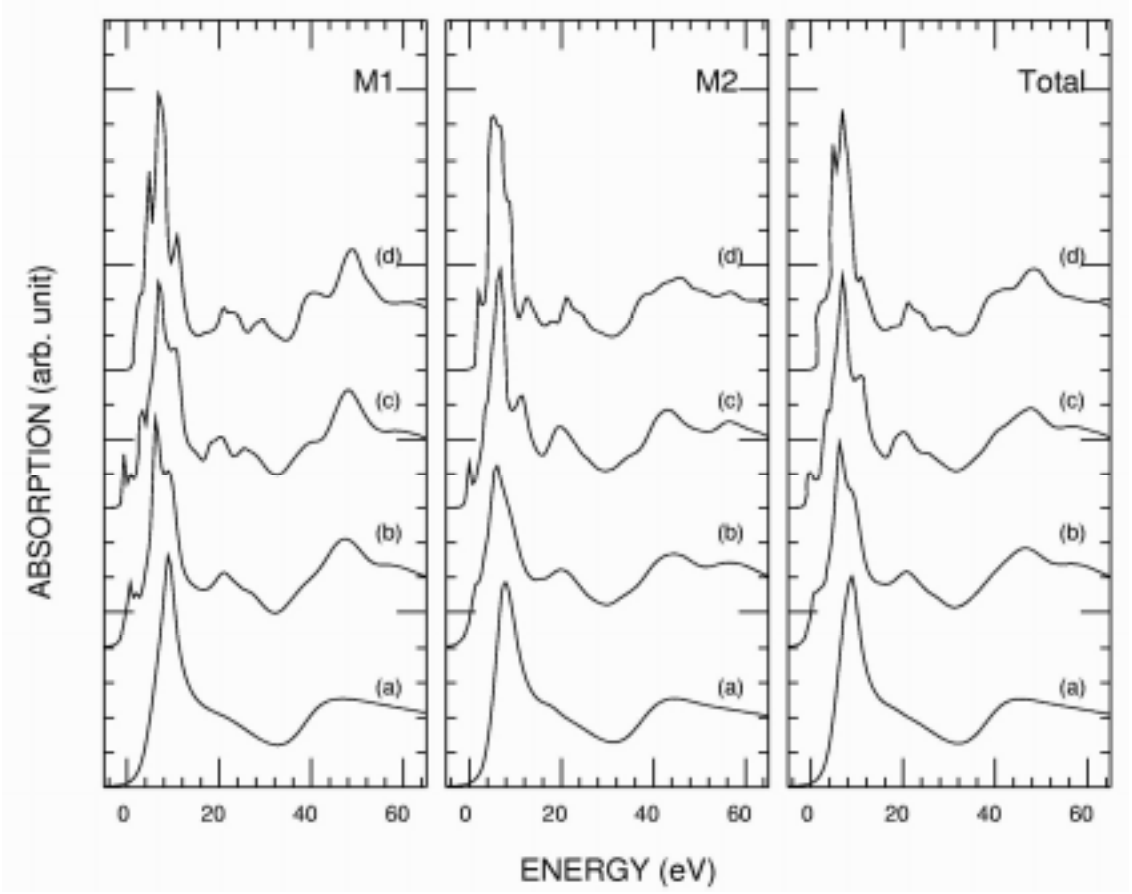

Figure 3 – Theoretical MS calculated spectra at the Mg K edge as a function of the cluster size for forsterite: the M1-site cluster (left panel), the M2-site cluster (central panel) and the summation of the two site contributions (right panel). Curves **a**, **b**, **c**, **d** refer to cluster calculations with increasing number of atoms: 7, 31, 55, and 89, respectively.

With increasing size of the two clusters built around the M1 and M2 sites (Fig. 3: curves **b**, **c**, and **d**), definite differences arise between the two calculated spectra which depend upon both the lengths of their bonds and their individual point symmetries. Such differences are not

so much to be seen in the FMS region of the spectra i.e., at the edge itself; rather, they show up best in the IMS region that, in this system, is located between 15 and 60 eV above threshold. In particular, the M1 convergent cluster spectrum (Fig. 3: left panel, curve **d**) has ripples that are more sharply defined than those occurring in the M2 convergent cluster spectrum (Fig. 3: middle panel, curve **d**). The M1 ripples are constantly displaced at higher energies than the corresponding ripples generated by clusters built around M2, thus confirming the inverse relationships between bond-length and energy known as Natoli's rule (Natoli and Benfatto 1986). Nevertheless, it would be difficult to deconvolute these individual contributions in experimental spectra.

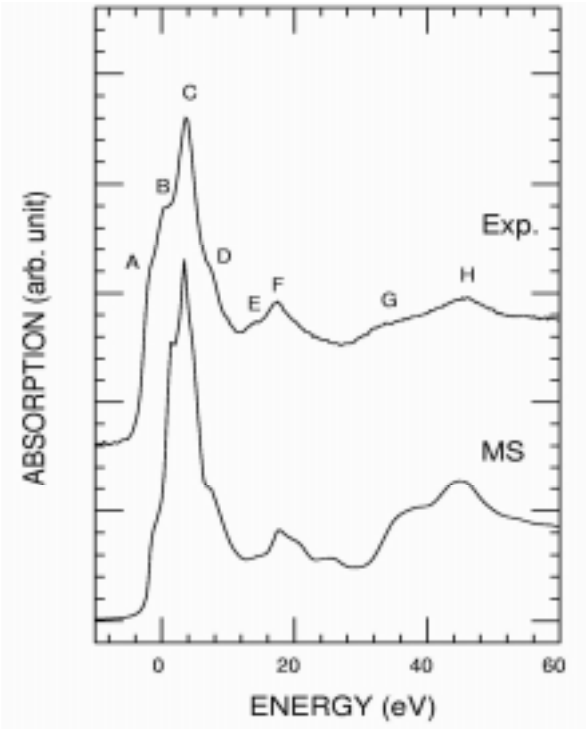

Figure 4 – Comparison of the MS calculated Mg K-edge spectrum of forsterite (after summation of two 89-atom clusters: Figure 3, right panel, curve **d**) with the experimental spectrum (Figure 1).

Actually, an experimental Mg K-edge XANES spectrum of forsterite consists of the superimposed contributions of all Mg atoms present in the structure i.e., of both clusters. Consequently, we performed a weighted combination of the calculated Mg-M1 and Mg-M2 convergent cluster spectra in the 1:1 proportion, as in the Fo stoichiometry. The summation results are shown in Fig. 3 (right panel), and a comparison between final and experimental spectra is given in Fig. 4. Not only the four gross features, but also all fine structures (now labeled individually from A to H) are well reproduced in their energies, with trifling discrepancies in their intensities: indeed, agreement is now much better than it was in our previous calculation (Wu et al. 1996a). In particular, all fine features in the IMS region are reproduced well. Comparison between experiment and theory shows that medium-range disorder is present in the measured material and significantly affects its spectrum by broadening (smoothing) particularly certain fine features. As these fine features appear to result from contributions from two types of octahedral sites, they cannot be of use as straightforwardly as hoped for our purpose of extracting all structural information they contain (see above), except in very special cases.

We also re-calculated the Fe K-edge spectrum of Fa in the same way i.e., for the two M1 and M2 clusters separately, as a function of their increasing size and using the Xα exchange potentials. This is not reported in all steps as for Fo because it matches even more closely with our previous calculation (Fig. 5 in Wu et al. 1996a). Note that at that time we had used for Fa Hazen's (1977) positional parameters instead of those by Fujino et al. (1981), and different exchange potentials. The fact that the results appear to be identical gives an indication of the accuracy of MS calculations performed by CONTINUUM. Indeed, it is our usual experience that, at energies as high as 7 KeV where the Fe K-edge is located, minor variations in the atomic parameters and potentials affect calculation very little. Consequently, in Fig. 5 (bottom) we only report the final Fa spectrum, obtained by adding the spectra of two convergent clusters containing 83 atoms each (29 Fe + 10 Si + 44 O) and extending to 0.59 nm away from center. It compares well with the experimental spectrum (Fig. 5, top), although it is sharper. Note, in particular, how the calculated pre-edge and white-line are both stronger than the experimental ones. We explain all this with the small difference in size that exists between the M1 and M2 octahedra, which makes their calculated contributions to shift so little as to overlap in the convolution. The fairly sharp spectra obtained by these calculations indirectly validate our view that the broad experimental spectra reported for some Fa (e.g., Waychunas et al. 1983; Calas et al. 1988) only reflect the poor quality of the analyzed sample or, in other words, a local to medium-range internal structural disorder acquired during synthesis and/or preparation.

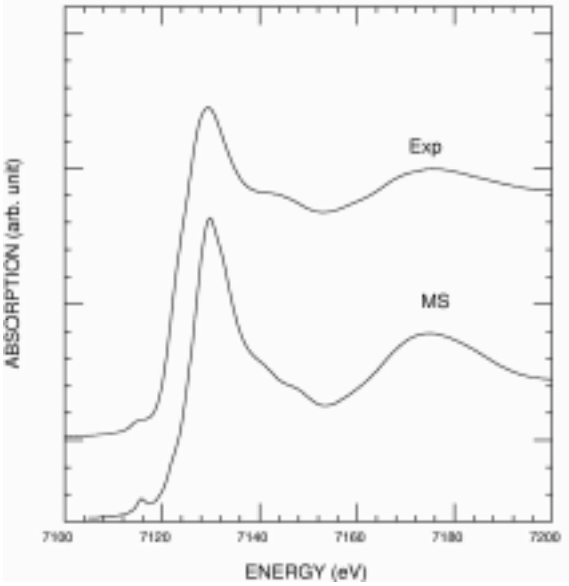

Figure 5 – Comparison of the MS calculated Fe K-edge spectrum of fayalite (after summation of the two 83-atom clusters centered on M1 and M2, respectively) with the experimental spectrum.

Fig. 6 and Fig. 7 show the Mg and Fe calculations performed for Mtc and Krs, respectively. In each case, we calculated only one sequence of clusters all centered around an M1 site that is fully occupied by Mg for Mtc and by Fe for Krs, assuming that Ca fills M2 alone.

For Mtc, the very first cluster calculation (Fig. 6 curve **a**) gives a first relevant feature centered at ca. +5 eV that is a doublet, possibly because of the slightly greater distortion of the Mtc octahedral M1 site with respect to the corresponding site of Fo (see above). There is also a feature at ca. +40 eV that reproduces the fourth gross one (F). Agreement progressively increases with the clusters including higher-shell atoms up to 55 (curve **c**). With further increase

(curve **d**) to a cluster that contains 99 atoms (15 Mg + 15 Si + 16 Ca + 53 O) and extends to 0.625 nm from the Mg absorber, calculated features become better defined, but with intensities more pronounced than in both the Fo case and the experimental spectrum (top). This new mismatch is to be explained with the generation of calculated pathways which do not exist in the measured sample. Thus, we consider agreement to be satisfactorily reached with a small cluster such as that containing 55 atoms (i.e., Fig. 8 curve **c**). The same compositional difference would explain the evident negative energy shift (-7 eV) between the fourth calculated feature and measured feature F. As for the intense feature A, that occurs in both the experimental and calculated spectra, we tend to attribute it to transition of the core electrons towards the 3p states that are empty in the Mg atom partly mixed with the empty density of states of the Ca atom located in the nearby M2 site (Wu et al. 1996b). We base our interpretation on the need of calculating spectra with clusters extending far beyond the first coordination sphere to attain matching even for the FSM region. This shows that this portion of the spectrum is sensitive jointly to the electronic structure as well as to the medium-range distribution of the atom acting as photoabsorber. So we cannot endorse the opinion that the final state reached in the core transitions is a simple atomic or molecular state (cf. de Groot et al. 1989; Li et al. 1993, 1995). Admittedly, our Mtc calculation of Fig. 6 reproduces the observed experimental features only qualitatively. Furthermore, it shows a series of fine structures in the IMS region (e.g., three around D) that are not observed in the experimental spectrum.
They may either originate from interactions with the very minor substitutions for Mg in M1 and Ca in M2 that are present in our natural sample (Table 1) or from the interactions of the photoelectron emitted by Mg in M1 directly with the Ca atoms in M2, these being located only some 0.32 nm away. In this case, they too would be indices of the same medium-range effects referred to above. In any case, they do not show up in the experimental spectrum because either our resolution is too low and experimental broadening too great or, possibly, because of the inhomogeneity of the sample.

The Krs calculated Fe K-edge spectrum (Fig. 7, bottom) compares unsatisfactorily with the experimental spectrum (Fig. 7, top), although to reach this result we had to make use of clever devices never used till now: (a) a rather large cluster, that extends to the seventh coordination shell and contains 109 atoms (15 Fe + 16 Ca + 16 Si + 62 O) to 0.68 nm away from the absorber; (b) a much greater Γ_{exp} (= 1.8 eV) during convolution. Such a need for large cluster and smooth potential speaks for local structural defects which had been either absent or averaged by SC-XRef in the meteoritic sample used as input (Folco and Mellini 1997), but which occur in our synthetic sample and are detected by XANES owing to its greater spatial resolution. The calculated major features (A and C in Fig. 2) have greater intensity, and shoulder B is less defined than in the experimental spectrum. Contrary to the Fa case (Fig. 5), there is no pre-edge in our calculation. We interpret this as meaning that the Fe pre-edge experimentally observed in Krs cannot derive from dipole-allowed transitions (as the Fa pre-edge could); it probably derives from quadrupole transitions, but this hypothesis should be confirmed by further theoretical analysis. In any case, the observed pre-edges are always too small and broad to be of any use to quantify the net valence of Fe (Bajt et al. 1994; Dyar et al. 1998), which is therefore taken as the conventional 2+. Furthermore, our Krs calculation is inadequate in that it

does not reproduce the hints for shoulder (arrows) that can be detected both on the low-energy limb of A and on the high-energy limb of B (Fig. 2). By contrast, the matched energy position for feature C indicates that the cluster size used for calculation is appropriate.

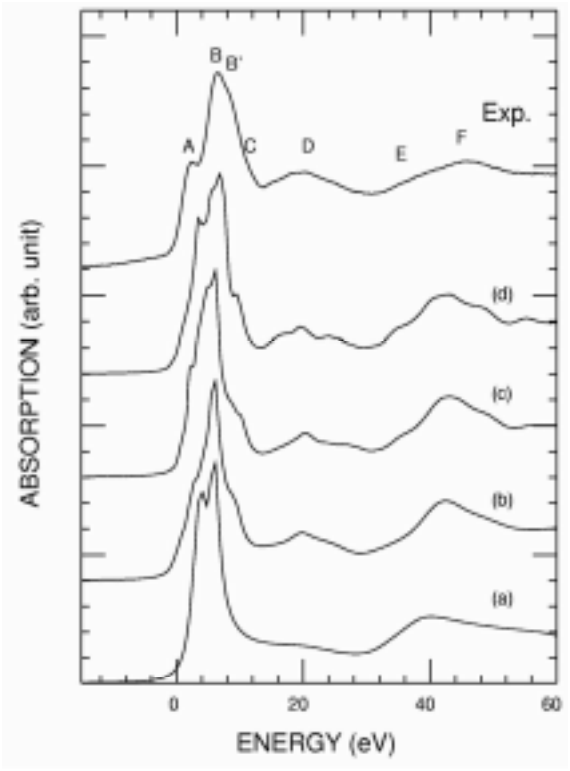

Figure 6 – Theoretical MS calculated spectra at the Mg K edge as a function of the cluster size for monticellite. Curves **a**, **b**, **c**, **d** refer to cluster calculations with increasing number of atoms: 7, 31, 55, and 99. The experimental spectrum is shown as the top curve.

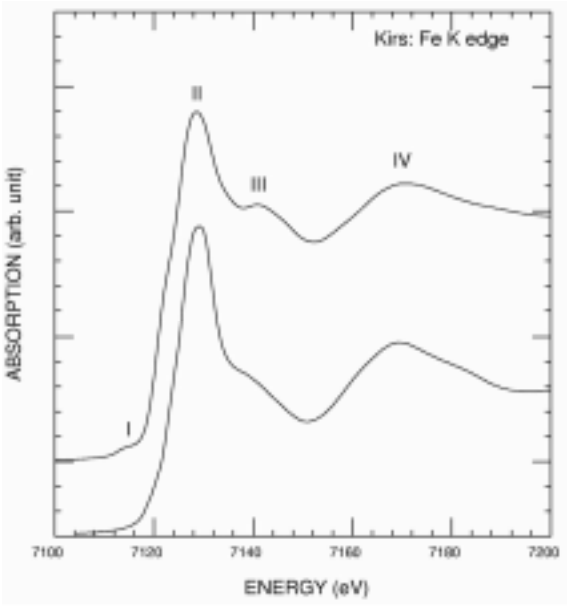

Figure 7 – Comparison of the MS calculated Fe K-edge spectrum of kirschsteinite (bottom) with the experimental spectrum (top).

Similar discrepancies affect the calculated Fe K-edge spectrum of "hortonolite", thus suggesting that the problem may be related not only to the electronic properties of the Fe atom, but also to its location in the structure. As a matter of fact, from SC-XRef it is not precisely known whether site M2 in Hrt is taken over only by Mg or Fe (and conversely for M1), or the two atoms intermix at random. Other methods, such as ME, also give conflicting evidence. This is indeed the problem with all intermediate olivines: are their solid solutions disordered, ordered or anti-ordered? And also: does order change with time because of factors such as cooling, or oxygen partial pressure, that affect olivines after crystallization?

Generally speaking, crystalline solution between divalent Fe-Mg silicate olivine endmembers is regular for most properties, both macro- and microscopic, and close to being ideal (e.g., Griffen 1992). There are exceptions for certain natural samples. E.g., the unit-cell parameters are linear functions of the radii of the octahedral M1 and M2 cations in synthetic olivines, but they may deviate considerably from linearity in natural olivines, particularly those of plutonic origin (Brown 1982; Hazen and Finger 1987; Motoyama and Matsumoto 1989;

Griffen 1992). These olivines trend to being ordered (or anti-ordered in the case that the large cation enters M1 instead of M2. Admittedly, such results always refer to LRO, because single-crystal diffraction methods can determine only it; yet all this is taken for granted in thermodynamic applications. However, the peculiar experimental features observed in our synthetic Hrt experimental Mg K-edge spectrum warn against hastily reaching the same conclusions when investigating the structure on a local scale, and rather suggest further checks that would take advantage of XANES property of selectively probing SRO.

In order to look for a satisfactory explanation of the peculiarities detected in the experimental Mg (and also Fe, but to a lesser extent) K-edge spectrum of our synthetic $MgFeSiO_4$ ("hortonolite") through an ordering model, we turned to simulation.

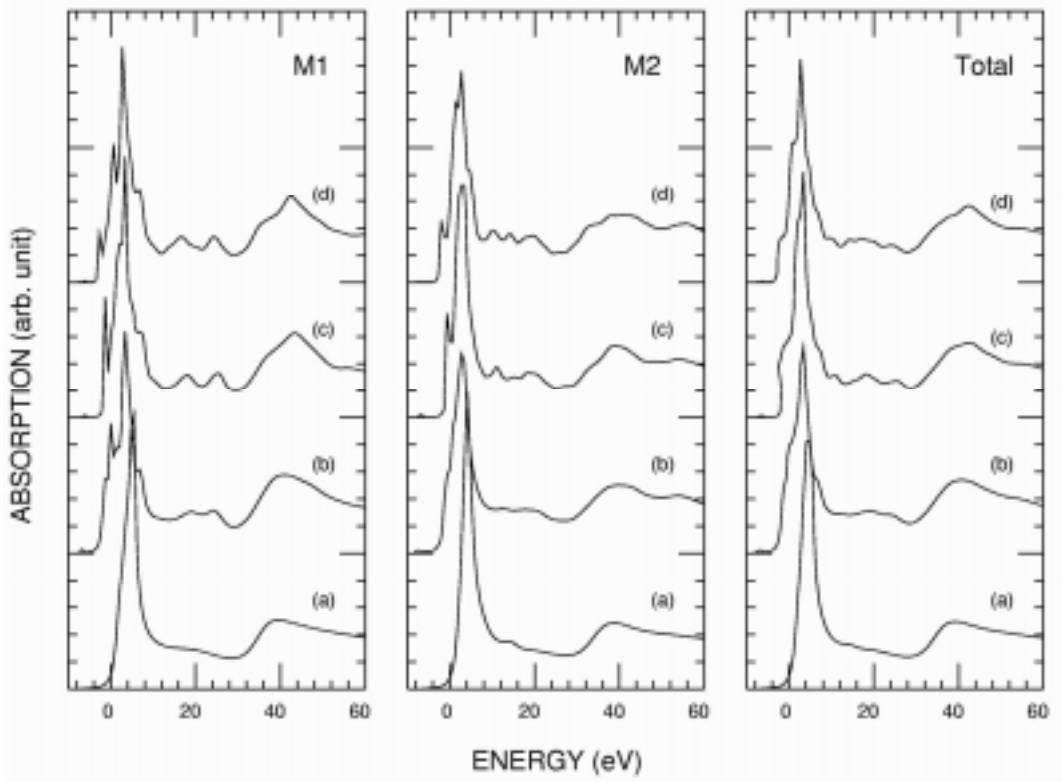

Figure 8 – Theoretical MS calculated spectrum simulations at the Mg K edge as a function of the cluster size for "hortonolite": the M1-site cluster when Mg is at M1 and Fe at M2 (left panel), the M2-site cluster when Mg is at M2 and Fe at M1 (central panel), and the summation of the two site contributions (right panel). Curves **a**, **b**, **c**, **d** refer to cluster calculations with increasing number of atoms: 7, 31, 55, and 85.

As our first model, we assumed that all Mg atoms are in M1 while all Fe atoms are in M2 i.e., we simulated the fully ordered distribution (Lumpkin and Ribbe 1983) and calculated the Mg K-edge spectra shown in Fig. 8 (left panel) as a function of cluster size (7, 31, 55, and 85 atoms, respectively). In all clusters beyond the very first one, we took care of maintaining as much as possible the 1:1 Mg:Fe stoichiometry. The first shell calculation (Fig. 8 curve **a**) obviously gives the same sharp and strong first peak (at +4 eV) and broad minor one at higher energy (+40 eV) as endmembers do. With increasing cluster size, and with the resulting increased interaction between Mg and Fe, two features arise at +15 and +25 eV that are due to the scattering contributions of atoms located in the third-order shell, 0.3~0.4 nm away from the

absorber (Fig. 8 curve **b**). They are similar to those seen when calculating Fo, but quite different from the broad band actually present in the experimental spectrum (Fig. 1). Further increases of the cluster size produce several sharp calculated fine structures on both sides of main feature A (Fig. 8 curves **c**, **d**) which resemble and may explain those seen in the experimental spectrum. However, agreement is far from being reached.

The middle panel of Fig. 8 shows the same series of cluster calculations, however performed according to the opposite model i.e., with Fe in M1 and Mg in M2 (the anti-ordered distribution: Lumpkin and Ribbe 1983). The final Mg K-edge calculated cluster spectrum (Fig. 8, middle curve **d**) appears to match the experimental spectrum better, although it is still far from being satisfactory. Fig. 8 (right panel) shows the convolution of the two sites contributions in the 1:1 proportion (i.e., in a fully random distribution of Mg and Fe over M1 and M2). Curve **d** is not yet in satisfactory agreement with the experimental spectrum (Fig. 1), especially for the medium-range IMS region between +15 and +25 eV. Clearly, further simulation is needed.

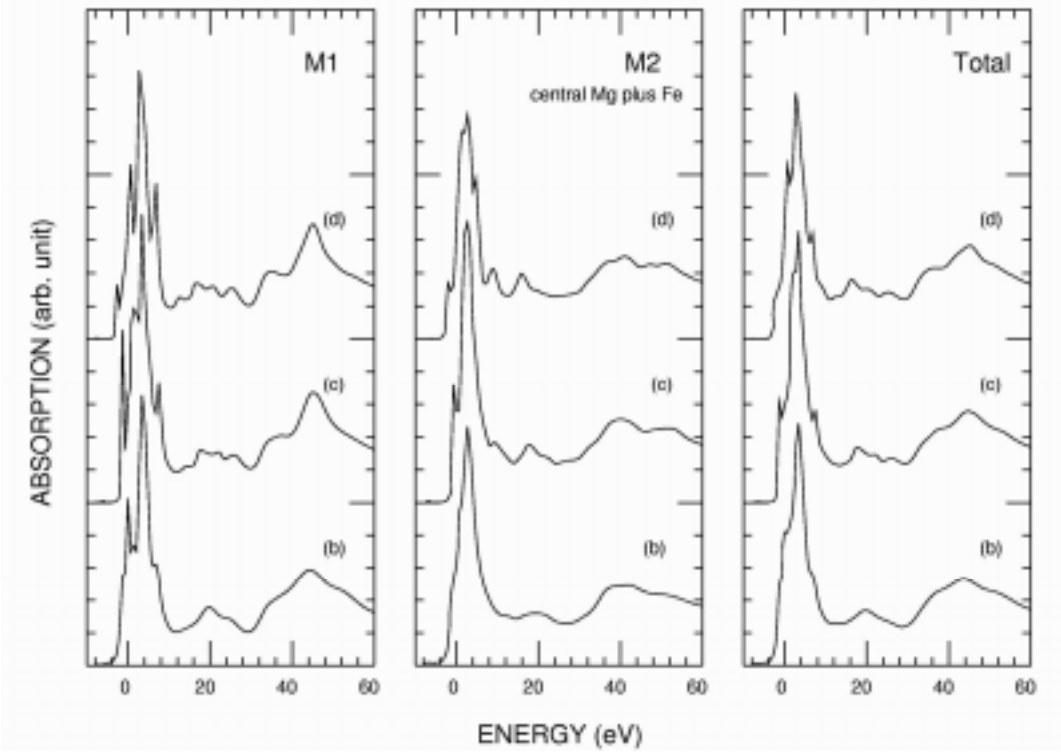

Figure 9 – Theoretical MS calculated spectrum simulations at the Mg K edge as a function of the cluster size for "hortonolite": the M1-site cluster in the case of a central M1-Mg surrounded by M1-Fe and with M2 occupied by Mg (left panel), the M2-site cluster in the case of a central M2-Mg surrounded by M2-Fe and with the M1 site occupied by Mg (central panel), and the convolution of the two site contributions (right panel). Curves **a**, **b**, **c**, **d** refer to cluster calculations with increasing number of atoms: 7, 31, 55, and 85.

Fig. 9 reports other theoretical simulations for "hortonolite" obtained by using clusters with the same number of atoms as the spectra in Fig. 8, but according to a new ordering model and with two alternative choices of site occupation. In the left panel, the Mg absorber is located in M1 and is surrounded by M1-Fe and M2-Mg. In the middle panel, the Mg absorber is in M2 and is surrounded by M1-Mg and M2-Fe. Calculations appear to match experiments better in

the first case than in the second one, and are also significantly better than those shown in Fig. 8, for both the FMS and IMS regions. Consequently, the spectrum obtained by summing up the two calculations (Fig. 9 curve **d,** right panel) appears to be in reasonable agreement with the experimental one.

So far, our calculations only indicate that in Hrt ordering of Fe and Mg over the M1 and M2 sites occurs. They also show that ordering can be simulated via calculations that test alternative possible distributions of the Fe and Mg atoms over the sites, although this painstaking procedure not always brings satisfactory results: as a matter of fact, even at the present stage it is impossible to conclude whether Fe is in M1 and Mg in M2, or vice versa.

To end our argument, in Fig. 10 we present three calculated Mg K-edge spectra and compare them with the experimental Mg XANES spectrum of "hortonolite". Curve **A** is the same as curve **d** in Fig. 8, right panel; curve **B** is curve **d** in Fig. 9, right panel; and curve **C** is the sum of **A** plus **B**. Only this theoretical spectrum reproduces all structures observed in the experimental spectrum (Fig. 10, top), however in their energy positions only, their relative

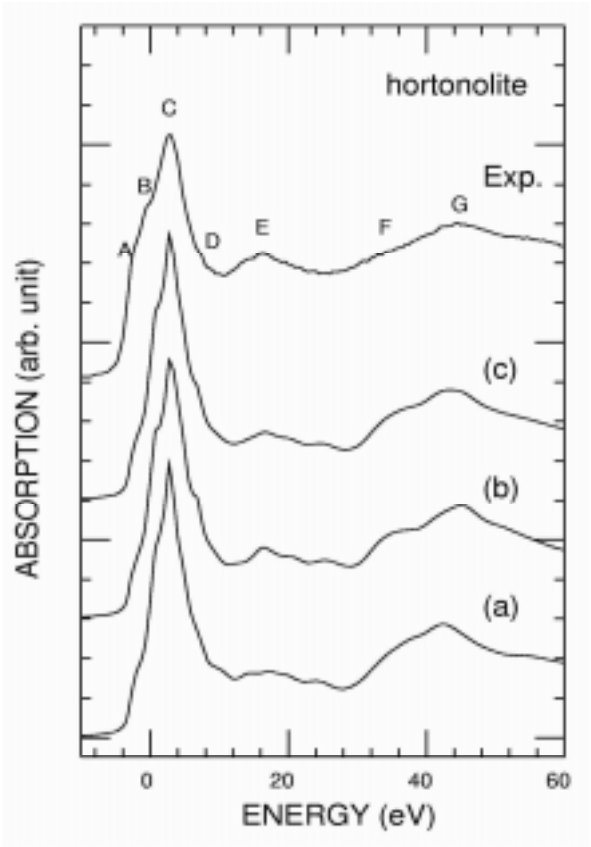

Figure 10 – Comparison of three MS simulated Mg K-edge spectra with the experimental spectrum of "hortonolite". Curve **A** is the same as **d** in the right panel of Figure 8; curve **B** comes from **d** in the right panel of Figure 9; curve **C** is the summation of **A** and **B**. See text for explanation

amplitudes being still in substantial disagreement. Furthermore, spectrum **C** shows a feature at +22 eV that cannot be seen in the experimental one. Another little mismatch is in that the experimental spectrum is somewhat broader than the calculated one, but this may be due to experimental reasons. From all these observation, we infer that our synthetic Hrt consists of a number of ordered domains each one characterized by its own type of Mg-Fe ordering. These domains are roughly in the 1:1 ratio and absorb simultaneously so as to produce the experimental spectrum by superimposing their individual contributions. Note that best

agreement between calculated and experimental features is to be found at the highest-energies, thus indicating that the chosen cluster size is correct and appropriate to both the experimental spectrum and the calculated one. The greater broadness of the experimental spectrum is a property that may be explained either by a greater amount of local disorder or a sort of modulation, by which slightly different octahedra centered by Mg and Fe periodically alternate along arrays in such a way as to allow the whole structure compensating their misfits and acquiring an overall order on a fairly long distance.

In order to crosscheck our study on Hrt, we should have performed a similar series of simulations for the Fe K edge. However, the experimental spectra shown in Fig. 2 suggest that such calculations would be a waste of effort: experimental resolution at 7.1 KeV is less than at 1.3 KeV and most fine structures become lost. This is why the Hrt experimental Fe K-edge spectrum (Fig. 2) appears to be simpler than the Mg K-edge one (Fig. 1) which displays such a large number of fine structures.

Ca K edges

In order to bring our study of the SRO structure of olivine minerals to completeness, in Fig. 11 we present the experimental Ca K-edge XANES spectra of monticellite and kirschsteinite, the two main calcian endmembers of the family. As already mentioned, it is a reasonable assumption that Ca segregates in the M2 site because of its large size. Nevertheless, there is positive SC-XRef evidence of it only for Mtc (Pilati et al. 1995 p. 723). For Krs, the problem is still open, essentially because the few samples refined so far were so impure as to suggest that the assumption could be taken for granted, and no tests made (Folco and Mellini 1997; Brown 1982 Table A4 p. 362).

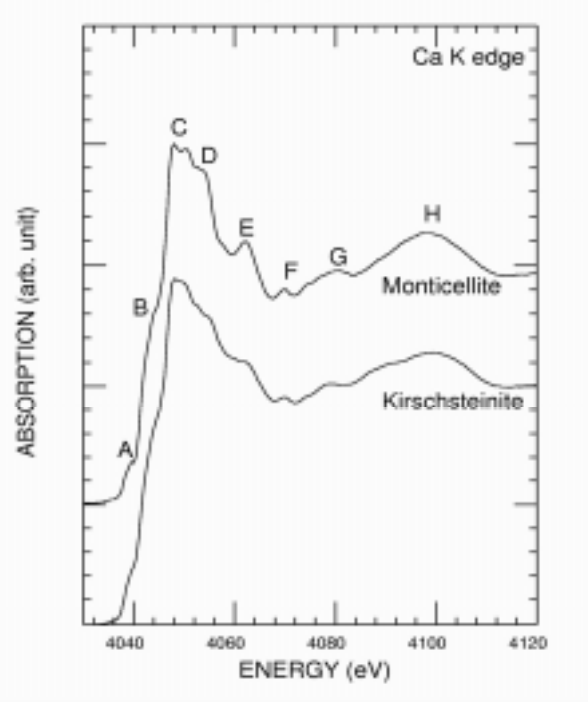

Figure 11 – Experimental Ca K-edge XANES spectra for monticellite and kirschsteinite

As a matter of fact, XANES studies support SC-XRef. The experimental Ca K-edge spectra of the two endmembers agree in almost all features (Fig. 11), Krs just being somewhat

less sharp than Mtc although being richer in fine structures. Minor differences are in the change of intensity of feature F, which turns from being a definite peak in Mtc to a shoulder in Krs, and in a broad feature to be seen in Krs (arrow) that would escape detection in Mtc because of its weakness, unless advised. These small discrepancies in the two spectra do not undermine the assignment of Ca entirely to M2. They only draw attention upon high-order effects that may arise from interaction of the photoelectron with heavy atoms, such as Fe.

Fig. 12 shows our theoretical MS calculated Ca K-edge spectra for Mtc and Krs obtained for clusters of increasing size up to the convergent ones containing 81 atoms each (11 Ca + 16 Fe/Mg + 12 Si + 42 O) and extending to 0.60÷0.61 nm from the M2 absorber i.e., the central Ca atom.

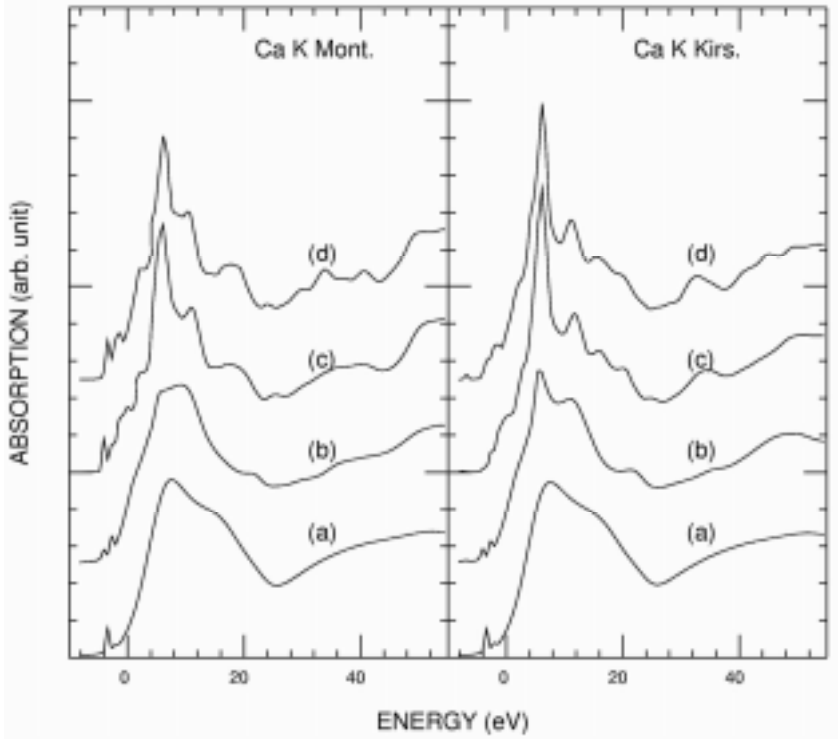

Figure 12 – Theoretical MS calculated spectra at the Ca K edge as a function of the cluster size for monticellite (left panel) and kirschsteinite (right panel). Curves **a**, **b**, **c**, **d** refer to cluster calculations with increasing number of atoms: 7, 24, 46, and 81.

The 7-atom cluster spectra are identical; they are fairly typical for any cation in an octahedral environment, but they are made conspicuous (compared with those of Mg and Fe) by the occurrence of small pre-edges and of a shoulder at +15 eV. The important characteristics begin to develop in the 24-atom clusters, which include second-shell atoms up to 0.40 nm away from the absorbers. Then, definite differences begin to appear between the two spectra which, nevertheless, fade away again when the clusters increase in size to encompass the third- and fourth-shell neighbors, i.e., at 0.51 and 0.61 nm. Further additions of more distant atoms (we calculated clusters with as many as 99 atoms, 0.65 nm in radius) no longer modify the calculated spectra. The convergent 81-atom cluster spectra duplicate the experimental ones reasonably well in the number of features (Fig. 11). However, they are consistently sharper than these are, thus suggesting that the natural materials that had been used for crystal structure refinement, in

addition to being of different composition, had their Ca atoms positionally more ordered than the samples we studied by XANES. Alternatively, the effect of experimental broadening could be called to attention. In any case, there is no evidence that Ca may move out of M2 to the M1 site.

CONCLUSIONS

By computing theoretical spectra on the basis of the one-electron full multiple-scattering theory starting from the atomic positional parameters determined by single-crystal X-ray diffraction refinement on the same or compositionally similar samples, we obtained an overall good agreement between calculation and experiment for the Ca, Mg and Fe K-edge XANES spectra of five olivine group minerals: forsterite (Fo), "hortonolite" (Hrt), fayalite (Fa), monticellite (Mtc), and kirschsteinite (Krs). All observed features could be replicated, both in their energies and relative intensities, albeit still with some differences in spectral resolution. By doing this:

1. we established, through cluster size construction, the volumes that can be probed by the X-ray absorption spectroscopy method in the energy range 1.3~7.1 KeV; indeed matching could be achieved only when using clusters containing at least 80 atoms i.e., as large as a sphere about 0.6 nm in radius around the absorber taken as the center of the cluster;
2. we could relate the different intensities of the main peaks in the full-multiple-scattering region (in particular of the first peak A) with the electronic properties of the probed atom i.e., the local character of the partially empty density of states. However, we could also show that medium-range contributions affect the edge region and modify it; this region is no longer to be seen only as a crude indicator of the valence and coordination of the probed atom;
3. we could show that most peaks in the intermediate-multiple-scattering region (in particular the low-intensity peaks D, E, and F) are related with the configurational properties of the system i.e., its crystal structure. Consequently, the mentioned sphere 0.6 nm in radius not only is the smallest volume that can be selectively probed by the photoelectron, but it is also the average volume of the crystal structure that can be integrated, explored, and interpreted by X-ray absorption spectroscopy (at least in the olivine system). Such a volume is three orders of magnitude smaller than any volume that would be scanned during a single-crystal X-ray diffraction refinement at the present time; in other words, XANES has a spatial resolution three orders of magnitude greater than XRD;
4. we have found evidence that "hortonolite", the intermediate member of olivine Mg-Fe solid solution series, is highly ordered on a local scale, but we have not found evidence that it has any significant preference for Fe viz. Mg in either site: we were only able to show by calculation that all models tested are inadequate to a certain extent. This result, albeit obtained for the moment on one sample only (furthermore: on a synthetic one), disputes previous conclusions reached on the basis of crystal structure refinements made by the X-ray diffraction method;
5. we could confirm that Ca segregates only in the M2 site of monticellite and kirschsteinite, thus supporting by an independent experimental method an inference based on the size of both atom and site that had been tested so far only cursorily.

These results confirm not only our confidence in the present state of calculation methods based on the one-electron full multiple-scattering theory for simulating XAS spectra, but also open the way to further applications of XANES to complex compounds and to other systems with variable degrees of order-disorder, hence resulting in detailed information on the partitioning of any selected atom over different sites to a level of spatial resolution unattainable by XRD.

ACKNOWLEDGEMENTS

This work was supported partly by EC Human Capital and Mobility grants (ZYW and GG) and partly by MURST grants under projects "Aspetti cristallochimici cinetici e termodinamici" (AM) and "Relazioni tra struttura e proprieta' dei minerali" (EP). Syntheses were carried out by GG at Bayerisches Geoinstitut Bayreuth thanks to the interest of D. Rubie and F. Seifert. Experiments at the Mg and Fe edges (proposal No. 2317) were done at SSRL, Stanford, which is operated by Stanford University on behalf of the US Department of Energy, Office of Basic Energy Science. Thanks are due to Michael Rowen, Jeff Moore, Curtis Troxel, Hal Tompkins and the entire SSRL staff for assistance. Experiments at the Ca K edge were done at LURE, Orsay, with the help of Isabella Ascone. Giuseppe Liborio provided natural samples, Francesco Demartin refined two structures, Maria Franca Brigatti calculated polyhedral distortions, Fernando Bartolomé and Jesús Chaboy recorded a spectrum and Antonio Grilli offered technical help. Critical readings by Maria Franca Brigatti, Rino Natoli, Brent Poe and Fritz Seifert are gratefully acknowledged. The remaining errors are only due to us.

REFERENCES

1. Aikawa N., Kumazawa M., and Tokonami M. (1985) Temperature dependence of intersite distribution of Mg and Fe in olivine and associated change of lattice parameters. Physics and Chemistry of Minerals, 12, 1-8.
2. Akamatsu T., Kumazawa M., Aikawa N., and Takei H. (1993) Pressure effect on the divalent cation distribution in nonideal solid solution of forsterite and fayalite. Physics and Chemistry of Minerals, 19, 431-444.
3. Alberti A. and Vezzalini G. (1978) Madelung energies and cation distribution in olivine type structures. Zeitschrift für Kristallographie, 147, 167-175.
4. Artioli G., Rinaldi R., Wilson C.C., and Zanazzi P.F. (1995) High-temperature Fe-Mg cation partitioning in olivine: in-situ single-crystal neutron diffraction study. American Mineralogist, 80, 197-200.
5. Bajt S., Sutton S.R., and Delaney J.S. (1994) Microanalysis of the iron oxidation states in silicates and oxides using X-ray absorption near-edge structure (XANES). Geochimica et Cosmochimica Acta, 58, 5209-5214.
6. Bianconi A. (1988) XANES spectroscopy. In D.C. Konigsberger & R. Prins, Eds., X-ray absorption: principles, applications, techniques of EXAFS, SEXAFS and XANES, pp. 573-662, Wiley, New York.
7. Brodholt J. (1997) Ab initio calculations on point defects in forsterite (Mg_2SiO_4) and implications for diffusion and creep. American Mineralogist, 82, 1049-1053.
8. Brown G.E. Jr. (1982) Olivines and silicate spinels. In P.H. Ribbe, Ed., Ortho-silicates, 2nd ed. Mineralogical Society of America Reviews in Mineralogy, 5, 275-381.
9. Brown G.E. Jr. and Prewitt C.T. (1973) High-temperature crystal chemistry of hortonolite. American Mineralogist, 58, 577-587.

10. Calas G., Manceau A., and Petiau J. (1988) Crystal chemistry of transition elements in minerals through X-ray absorption spectroscopy. In S.S. Augustithis, Ed., Synchrotron radiation applications in mineralogy and petrology, pp. 77-95, Theophrastus, Athens.
11. Chakraborty S. (1997) Rates and mechanisms of Fe-Mg interdiffusion in olivine at 980°-1300°C. Journal of Geophysical Research, 102, 12317-12331.
12. Clementi E. and Roetti C. (1974) Nuclear Data Tables, 14 [3-4], 177-478. Academic Press, New York.
13. Durham P.J. (1988) X-ray absorption. In D.C. Konigsberger and R. Prins, Eds., X-ray absorption: principles, applications, techniques of EXAFS, SEXAFS and XANES, pp. 53-84, Wiley, New York.
14. Durham P.J., Pendry J.B., and Hodges C.H. (1982) Calculation of X-ray absorption near-edge structure, XANES. Computer Physical Communications, 25, 193-205.
15. Dyar M.D., Delaney J.S., Sutton S.R., and Schaefer M.W. (1998) Fe^{3+} distribution in oxidized olivine: a synchrotron micro-XANES study. American Mineralogist, 83, 1361-1365.
16. Erbil A., Cargill E.S. III, Frahm R., and Boehme R.F. (1988) Total-electron-yield current measurements for near-surface extended x-ray-absorption fine structure. Physical Review, B 37, 2450-2464.
17. Folco L. and Mellini M. (1997) Crystal chemistry of meteoritic kirschsteinite. European Journal of Mineralogy, 9, 969-973.
18. Fuggle J.C. and Inglesfield J.E. (1992) Unoccupied electronic states. Fundamentals for XANES, EELS, IPS and BIS. Springer, Berlin.
19. Fujino K., Sasaki Y., Takéuchi Y., and Sadanaga R. (1981) X-ray determination of electron distribution in forsterite, fayalite and tephroite. Acta Crystallographica, B 37, 513-518.
20. Galoisy L. and Calas G. (1992) Network-forming Ni in silicate glasses. American Mineralogist, 77, 677-680.
21. Griffen, D.T. (1992) Silicate crystal chemistry. Oxford University Press, New York & Oxford.
22. Groot F.M.F. de, Grioni M., Fuggle J.C., Ghijsen J., Sawatzky G.A., and Petersen H. (1989) Oxygen 1s x-ray-absorption edges of transition-metal oxides. Physical Review, B 40, 5715-5723.
23. Gudat W. and Kunz C. (1977) Close similarity between photoelectric yield and photoabsorption spectra in the soft-X-ray range. Physical Review Letters, 29, 169-172.
24. Hazen R.M. (1977) Effects of temperature and pressure on the crystal structure of ferromagnesian olivine. American Mineralogist, 62, 286-295.
25. Hazen R.M. and Finger L.W. (1987) Comparative crystal chemistry. Wiley, New York.
26. Hedin L. and Lundqvist B.I. (1971) Explicit local exchange-correlation potentials. Journal de Physique, C 4, 2064-2083.
27. Henderson C.M.B., Knight K.S., Redfern S.A.T., and Wood B.J. (1996) High-temperature study of cation exchange in olivine by neutron powder diffraction. Science, 271, 1713-1715.
28. Hofmeister A.M. (1987) Single-crystal absorption and reflection infrared spectroscopy of forsterite and fayalite. Physics and Chemistry of Minerals, 14, 499-513.
29. Iishi K. (1978) Lattice dynamics of forsterite. American Mineralogist, 63, 1198-1208.
30. Kieffer S.W. (1979) Thermodynamics and lattice vibration of minerals: 1. Mineral heat capacities and their relationships to simple lattice vibrational models. Reviews of Geophysics and Space Physics, 17, 1-19.
31. Kirfel, A. (1996) Cation distributions in olivines and orthopyroxenes. An interlaboratory study. Physics and Chemistry of Minerals, 23, 503-519.
32. Krause M.O. and Oliver J.H. (1979) Natural widths of atomic K and L levels, Kα X-ray lines and several KLL Auger lines. Journal of Physical Chemical Reference Data, 8, 329-338.
33. Kurata H., Lefevre E., Cilliex C., and Brydson R. (1993) Electron-energy-loss near-edge structures in the oxygen K-edge spectra of transition-metal oxides. Physical Review, B 47, 13763-13768.

34. Lee P.A. and Beni G. (1977) New method for the calculation of atomic phase shifts: application to extended x-ray absorption fine structure (EXAFS) in molecules and crystals. Physical Review, B 15, 2862-2883.
35. Lee P.A. and Pendry J.B. (1975) Theory of the extended x-ray absorption fine structure. Physical Review, B 11, 2795-2811.
36. Li D., Bancroft G.M., Kasrai M., Fleet M.E., Feng X.H., Tan K.H., and Yang B.X. (1993) High-resolution Si K- and $L_{2,3}$-edge XANES of α quartz and stishovite. Solid State Communications, 87, 613-617.
37. Li D., Bancroft G.M., Fleet M.E., Feng X.H., and Pan Y. (1995) Al K-edge spectra of aluminosilicate minerals. American Mineralogist, 80, 432-440.
38. Lindner Th., Sauer H., Engel W., and Kambe K. (1986) Near-edge structure in electron-energy-loss spectra of MgO. Physical Review, B 33, 22-24.
39. Lumpkin G.R. and Ribbe P.H. (1983) Composition, order-disorder and lattice parameters of olivines: relationships in silicate, germanate, beryllate, phosphate and borate olivines. American Mineralogist, 68, 164-176.
40. Lumpkin G.R., Ribbe P.H., and Lumpkin N.E. (1983) Composition, order-disorder and lattice parameters of olivines: determinative methods for Mg-Mn and Mg-Ca silicate olivines. American Mineralogist, 68, 1174-1182.
41. Lytle F.W., Greegor R.B., Sandstrom D.R., Marques E.C., Wong J., Spiro C.L., Huffman G.P., and Huggins F.E. (1984) Measurement of soft x-ray absorption spectra with a fluorescence ion chamber detector. Nuclear Instruments and Methods in Physical Research, A 226, 542-548.
42. Mattheiss L. (1964) Energy bands for the iron transition series. Physical Review, A 134, 970-975.
43. Miller M.L. and Ribbe P.H. (1985) Methods for determination of composition and intracrystalline cation distribution in Fe-Mn and Fe-Ni silicate olivines. American Mineralogist, 70, 723-728.
44. Motoyama T. and Matsumoto T. (1989) The crystal structure and the cation distributions of Fe and Mg of natural olivines. Mineralogical Journal, 14, 338-350.
45. Mottana A., Murata T., Wu Z.Y., Marcelli A., and Paris E. (1997) The local structure of Ca-Na pyroxenes. I. XANES study at the Na K-edge. Physics and Chemistry of Minerals, 24, 500-509.
46. Mottana A., Murata T., Marcelli A., Wu Z.Y., Cibin G., Paris E., and Giuli G. (1999) The local structure of Ca-Na pyroxenes. II. XANES studies at the Mg and Al K edges. Physics and Chemistry of Minerals (in press).
47. Muller O. and Roy R. (1974) The major ternary structure families. Springer, New York.
48. Nakamura A. and Schmalzried H. (1983) On the non-stoichiometry and point defects of olivine. Physics and Chemistry of Minerals, 10, 27-37.
49. Natoli C.R. and Benfatto M. (1986) A unifying scheme of interpretation of X-ray absorption spectra based on the multiple scattering theory. Journal de Physique, C 8, 47, 11-23.
50. Natoli C.R., Misemer D.K., Doniach S., and Kutzler F.W. (1980) First-principles calculation of X-ray absorption-edge structure in molecular cluster. Physical Review, B 22, 1104-1108.
51. Natoli C.R., Benfatto M., Brouder C., Ruiz Lopez M.Z., and Foulis D.L. (1990) Multichannel multiple-scattering theory with general potentials. Physical Review, B 42, 1944-968.
52. Norman J.G. (1974) Non-empirical versus empirical choices for overlapping-sphere radii ratios in SCF-Xα-SW calculations on ClO_4- and SO_2. Molecular Physics, 31, 1191 -1198.
53. Ottonello G. (1987) Energies and interactions in binary (Pbnm) orthosilicates: a Born parametrization. Geochimica et Cosmochimica Acta, 51, 3119-3135.
54. Ottonello G., Princivalle F., and Della Giusta A. (1990) Temperature, composition, and *f*o2 effects on intersite distribution of Mg and Fe^{2+} in olivines. Experimental evidence and theoretical interpretation. Physics and Chemistry of Minerals, 17, 301-312
55. Penn D.R. (1987) Electron mean-free-path calculations using a model dielectric function. Physical Review, B 35, 482-486.

56. Pilati T., Bianchi R., and Gramaccioli C.M. (1990) Lattice-dynamical estimation of atomic thermal parameters for silicates: forsterite α-Mg_2SiO_4. Acta Crystallographica, B 46, 301-311.
57. Pilati T., Demartin F., and Gramaccioli C.M. (1995) Thermal parameters for minerals of the olivine group: their implication on vibrational spectra, thermodynamic functions and transferable force fields. Acta Crystallographica, B 51, 721-733.
58. Poirier J.-P. (1991) Introduction to the physics of the Earth's interior. Cambridge University Press, Cambridge.
59. Redfern S.A.T., Henderson C.M.B., Wood B.J., Harrison R.J., and Knight K.S. (1996) Determination of olivine cooling rates from metal-cation ordering. Nature, 381, 407-409.
60. Rez P., Bruley J., Bohan P., Payne M., and Garvie L.A.J. (1995) Review of methods for calculating near edge structure. Ultramicroscopy, 59, 159-167.
61. Robinson K., Gibbs G.V., and Ribbe P.H. (1971) Quadratic elongation: a quantitative measure of distortion in coordination polyhedra. Science, 172, 567-570.
62. Schaefers F., Müller B.R., Wong J., Tanaka T., and Kamimura Y. (1992) YB_{66}: a new soft X-ray monochromator crystal. Synchrotron Radiation News, 5 [2], 28-30.
63. Sharp Z.D., Hazen R.M., and Finger L.W. (1987) High-pressure crystal chemistry of monticellite, $CaMgSiO_4$. American Mineralogist, 72, 748-755.
64. Slater J.C. (1979) Quantum theory of molecules and solids. McGraw-Hill, New York.
65. Smyth J.R. and Hazen R.M. (1973) The crystal structures of forsterite and hortonolite at several temperatures up to 900 °C. American Mineralogist, 58, 588-593.
66. Tracy R.J. and Frost B.R. (1991) Phase equilibria and thermobarometry of metapelites. In D.M. Kerrich, Ed., Contact metamorphism. Mineralogical Society of America Reviews in Mineralogy, 26, 207-290.
67. Tyson T.A., Hodgson K.O., Natoli C.R., and Benfatto M. (1992) General multiple-scattering scheme for the computation and interpretation of x-ray absorption fine structure in atomic clusters with application to SF_6, $GeCl_4$ and Br_2 molecules. Physical Review, B 46, 5997-6019.
68. Valley J.W. and Essene E.J. (1980) Akermanite in the Cascade Slide xenolith, and its significance for regional metamorphism in the Adirondacks. Contributions to Mineralogy and Petrology, 74, 143-152.
69. Virgo D. and Hafner S.S. (1972) Temperature dependent Mg,Fe distribution in lunar olivine. Earth and Planetary Science Letters, 14, 305-312.
70. Vvedensky D.D. and Pendry J.B. (1985) Comment on "Experimental study of multiple scattering in X-ray-absorption near-edge structure". Physical Review Letters, 54, 2725-2726 (1985).
71. Waychunas G.A., Brown G.E. Jr., and Apted M.J. (1983) X-ray K-edge absorption spectra of Fe minerals and model compounds: near edge structure. Physics and Chemistry of Minerals, 10, 1-9.
72. Williams Q., Knittle E., Reichlin R., Martin S., and Jeanloz R. (1990) Structural and electronic properties of Fe_2SiO_4-fayalite at ultrahigh pressures: amorphization and gap closure. Journal of Geophysical Research, 95, B13, 21549-21563.
73. Wong J., George G.N., Pickering I.J., Rek Z.U., Rowen M., Tanaka T., Via G.H., DeVries B., Vaughan D.E.W., Brown G.E. Jr. (1994) New opportunities in XAFS investigation in the 1-2 keV region. Solid State Communications, 92, 559-562.
74. Wu, Z.Y., Mottana A., Marcelli A., Natoli C.R., and Paris E. (1996a) Theoretical analysis of X-ray absorption near-edge structure in forsterite, Mg_2SiO_4-Pbnm, and fayalite, Fe_2SiO_4-Pbnm, at room temperature and extreme conditions. Physics and Chemistry of Minerals, 23, 193-204.
75. Wu Z.Y., Marcelli A., Mottana A., Giuli G., Paris E., and Seifert F. (1996b) Effects of higher-correlation shells in garnets detected by x-ray-absorption spectroscopy at the Al *K* edge. Physical Review, B 54, 2976-2979.